A R C H I V E O F M E C H A N I C A L E N G I N E E R I N G

Volume 67 2020 Number 4

DOI: 10.24425/ame.2020.131701

Key words: human cochlea, basilar membrane, unsteady viscous fluid flow, fluid-structure interaction, pressure-displacement-based fluid element, viscous boundary layer, tonotopy, auditory threshold

Philipp Wahl[1], Pascal Ziegler[1], Peter Eberhard [1]

Numerical investigation of the basilar membrane vibration induced by the unsteady fluid flow in the human inner ear

For a deeper understanding of the inner ear dynamics, a Finite-Element model of the human cochlea is developed. To describe the unsteady, viscous creeping flow of the liquid, a pressure-displacement-based Finite-Element formulation is used. This allows one to efficiently compute the basilar membrane vibrations resulting from the fluid-structure interaction leading to hearing nerve stimulation. The results show the formation of a traveling wave on the basilar membrane propagating with decreasing velocity towards the peaking at a frequency dependent position. This tonotopic behavior allows the brain to distinguish between sounds of different frequencies. Additionally, not only the middle ear, but also the transfer behavior of the cochlea contributes to the frequency dependence of the auditory threshold. Furthermore, the fluid velocity and pressure fields show the effect of viscous damping forces and allow us to deeper understand the formation of the pressure difference, responsible to excite the basilar membrane.

1. Introduction

The human inner ear or cochlea is a bone structure of spiral shape and is composed of mainly two conical chambers which are filled with fluid and separated by a soft membrane, referred to as the basilar membrane. At the apical end, both chambers are connected through a small opening, the helicotrema. At the base, the chambers are closed by the stapes footplate and the round window membrane, respectively. In case of a normal ear, sound is received by the eardrum and transmitted to the cochlea through the middle ear ossicles. According to present hearing theory, the vibration of the stapes footplate leads to pressure waves in the cochlear

✉ Peter Eberhard: peter.eberhard@itm.uni-stuttgart.de

[1]Institute of Engineering and Computational Mechanics, University of Stuttgart, Pfaffenwaldring 9, 70569 Stuttgart, Germany.

© 2019. The Author(s). This is an open-access article distributed under the terms of the Creative Commons Attribution-NonCommercial-NoDerivatives License (CC BY-NC-ND 4.0, https://creativecommons.org/licenses/by-nc-nd/4.0/), which permits use, distribution, and reproduction in any medium, provided that the Article is properly cited, the use is non-commercial, and no modifications or adaptations are made.

www.czasopisma.pan.pl PAN POLSKA AKADEMIA NAUK www.journals.pan.pl

fluid, which in turn results in a characteristic vibration of the basilar membrane. Related to the sound frequency, hair cells in certain areas of the basilar membrane are stimulated, causing hearing nerve stimulation and, thus, leading to hearing sensation.

In order to predict the effect of inner ear diseases on hearing sensation as well as to develop new hearing implants, a deeper understanding of the cochlear dynamics is needed. This is particularly important, since the cochlea represents a closed hydraulic system with a complex geometry. The basilar membrane vibration as well as the fluid pressure can only be measured locally in the basal domain by conducting very elaborate experiments on temporal bone specimens of humans or animals [1]. However, simulations with an adequate numerical model of the inner ear allow one to study the characteristic basilar membrane vibration and the cochlear fluid dynamics along the entire length of the hearing organ and thus provide an insight into the fundamental physical effects occurring in this system.

Therefore, in this study a Finite-Element (FE) model of the uncoiled human cochlea is developed. Here, only the passive properties are modeled, i.e., the cochlea is modeled without considering amplification by electro-mobility of the outer hair cells. In the first part of this paper, the simplified field equations to describe the oscillating fluid flow in the cochlea are presented. The differential equations are discretized by the use of the Finite-Element Method and an adequate formulation of the fluid-structure interaction is described. The user-defined element for the fluid is briefly validated for a coupled system by comparing the calculated frequency response of an oscillating beam in a viscous fluid with the corresponding analytical solution. Then, the geometry and material properties for the cochlea model are described with a particular focus on the material description for the basilar membrane. According to the membrane's anatomical structure, the membrane can be divided into two zones, for which different material descriptions will be presented.

In the second part of this paper, the calculated basilar membrane vibration as well as the fluid velocity and pressure fields are discussed. The simulation results show the formation of a traveling wave on the basilar membrane. The amplitude of this wave increases from the base towards the apex and peaks at a frequency dependent location. This so-called tonotopic behavior then allows the brain to distinguish sounds of different frequencies. Furthermore, it can be shown, that not only the transfer behavior of the middle ear, but also that of the cochlea contributes to the frequency dependency of the human auditory threshold. Investigating the computed fluid velocity field in the thin viscous boundary layer close to the basilar membrane, the damping mechanism leading to this traveling wave is identified. Additionally, the results show that the cochlear fluid flow is strongly unsteady and viscous. Further, the calculated pressure distribution in the fluid-filled chambers is analyzed and indicates that the pressure is amplified from the ear canal to the inner ear. Additionally, the pressure difference across the basilar membrane, which evokes the characteristic basilar membrane vibration, results from the unsteady inertia forces rather than from the compression of the fluid.

www.czasopisma.pan.pl PAN POLSKA AKADEMIA NAUK www.journals.pan.pl

Consequently, the novel contribution of this paper compared to previous studies can be summarized as follows: the pressure-displacement-based, viscous fluid formulation is so far mainly used for sub-models in order to study the fluid flow around hair bundles [2, 3]. However, in this paper, the fluid description is applied in a developed two-box model of the entire cochlea. This allows us to simulate and investigate the velocity and pressure fields in the fluid close to the basilar membrane. It can be shown that in these fluid boundary layers significant viscous forces are present acting, due to the fluid-structure interaction, on the basilar membrane. This in turn then leads to the formation of the characteristic traveling wave resulting in hearing nerve stimulation. Therefore, viscous forces have to be captured in cochlear modeling. However, in most FE-models fluid elements as acoustic elements or simplified displacement-based fluid elements are used partly or completely neglecting these forces already in the underlying fluid equations [4, 5]. Then, arbitrary defined impedance surfaces in the fluid domain or spatial distributions of structural damping coefficients for the basilar membrane are applied in order to introduce sufficient damping to the cochlea model. However, this approach can be regarded as a numerical approximation of the resulting basilar membrane vibration pattern, rather than physical modeling, as it is presented in this study. Further, the fluid description applied here allows us to efficiently compute the cochlear fluid-structure interactions in the frequency domain. This is in contrast to the commonly-used partitioned approach often resulting in numerical instabilities during the time-consuming co-simulation.

In order to accurately describe the traveling wave on the basilar membrane, not only the fluid formulation, but also the material description of the membrane plays a significant role. Although experimental findings clearly indicate that the basilar membrane is, based on its morphologic structure, divided into two different zones, in most existing FE-models an isotropic material formulation for the entire membrane is used, e.g., [6]. Then, usually material parameters are fitted with respect to tonotopy resulting in questionably high Young's moduli. However, this is in contradiction to the morphologic structure of the pectinate zone with its radially-orientated bands [7–9]. Therefore, in this study, for this zone an orthotropic material formulation is applied resulting in a two-zone material description for the basilar membrane.

Both, the applied fluid description and the presented material formulation for the basilar membrane then allow one to accurately simulate with the developed FE-model, the fundamental physical effects occurring in the human cochlea. The simulation of the characteristic basilar membrane vibration and the fluid flow in the human cochlea makes it possible to identify the mechanism for the excitation and formation of the traveling wave on the basilar membrane. Since the vibration of this membrane in turn leads to hearing nerve stimulation, the investigations provide a deeper understanding for the generation of the resulting hearing sensation. Further, the calculated transfer behavior for the basilar membrane demonstrates the tonotopic organization of the human cochlea and thus clarifies the capability of

www.czasopisma.pan.pl PAN POLSKA AKADEMIA NAUK www.journals.pan.pl

the human inner ear to distinguish sounds of different frequencies. Additionally, the results point out that the cochlear transfer behavior itself contributes to the frequency dependence of the auditory threshold.

2. Method

The oscillating fluid flow in the cochlea is induced by the vibration of the stapes footplate. In contrast to classical engineering flow problems, the oscillatory fluid motions are small and, therefore, the nonlinearities resulting from large deformations can be neglected. This allows colorredone to simplify the field equations for the fluid to a linear set of equations in terms of displacement. In this way, an efficient calculation of the cochlear fluid-structure interaction in the frequency domain is achieved, as shown in the following.

2.1. Field equations for the fluid

In a first step, the kinematics for infinitesimal strains and the material description for the fluid are incorporated into the general conservation equations [10, 11]. Then, these equations are simplified for the flow in the inner ear by use of dimensionless numbers [3]. In this way, the field equations for the fluid, which is treated here as a viscous and compressible liquid, are derived.

The fluid displacement amplitudes are small compared to the geometry of the cochlea. Thus, the dimensionless Keulegan-Carpenter number [12] is below one, and the continuity equation in an Eulerian frame simplifies to

$$\frac{\partial \rho_\mathrm{f}}{\partial t} = 0 \tag{1}$$

with the fluid density ρ_f and the time t.

The momentum equation contains the surface forces and the external body forces. In order to describe the surface forces, the relation between the state of stress and the state of deformation of the fluid is required. This link is given by the material description. Since the material properties of the inner ear fluid are similar to a salt-water solution [13, 14], the liquid is treated as a Newtonian fluid. Thus, the stress tensor can be described by the dynamic viscosity η_f and the strain-rate tensor. In contrast to many engineering flow problems, the fluid flow in the cochlea is charaterized by low fluid velocities and small geometric dimensions. Therefore, the Reynolds number is below one [15] and the nonlinear convective term in the momentum equation can be omitted. However, the vibration of the stapes footplate leads to an oscillating fluid flow and, thus, the dimensionless Womersley number is large [15]. Therefore, the inertial term is retained. Neglecting external body forces, the resulting linear momentum equation reads

$$-\nabla p_\mathrm{f} + \eta_\mathrm{f} \nabla \cdot \left(\nabla \mathbf{v}_\mathrm{f} + (\nabla \mathbf{v}_\mathrm{f})^T - \frac{2}{3} \nabla \cdot \mathbf{v}_\mathrm{f} \mathbf{I} \right) = \rho_\mathrm{f} \frac{\partial \mathbf{v}_\mathrm{f}}{\partial t} \tag{2}$$

www.czasopisma.pan.pl PAN POLSKA AKADEMIA NAUK www.journals.pan.pl

with the fluid pressure p_f, velocity $\mathbf{v}_\mathrm{f} = [u_\mathrm{f}, v_\mathrm{f}, w_\mathrm{f}]^T$ and second-order identity tensor $\mathbf{I}$.

For the energy equation, external heat sources and body forces are neglected and the field equation is written in terms of the fluid temperature T_f. Applying the Fourier approach [16], this allows us to link the heat flux vector with the temperature field through the thermal conductivity λ_th of the liquid. The stress tensor is again described by the fluid viscosity and the strain-rate tensor assuming a Newtonian fluid. According to the momentum equation, the inertial term is proportional to the large Womersley number and, therefore, has to be retained, whereas the convective term is dropped due to the low Reynolds number. Further, the low fluid velocities lead to a low kinetic energy of the fluid and result in a very small Eckert number. Therefore, the unsteady pressure variations, their convective transport, and the thermal energy resulting from viscous losses are omitted. Additionally, the material properties for the inner ear fluid lead to a dimensionless Prandtl number well above one. Hence, the thermal-dissipative term, which scales with the reciprocal value of this number is neglected and the energy equation simplifies to

$$\frac{\partial T_\mathrm{f}}{\partial t} = 0. \tag{3}$$

The continuity equation (1) and the energy equation (3) show that the density and temperature of the fluid flow in the cochlea are constant in time. The momentum equation (2) contains the variables pressure and velocity. Dealing with small amplitudes in the field of cochlear mechanics, the velocity is replaced by the time derivative of the displacement. The missing link between the variable pressure and displacement provides the constitutive equation for a Newtonian fluid. The final set of field equations for the fluid then reads

$$-\nabla p_\mathrm{f} + \eta_\mathrm{f}\nabla\cdot\left(\nabla\frac{\partial \mathbf{u}_\mathrm{f}}{\partial t} + \left(\nabla\frac{\partial \mathbf{u}_\mathrm{f}}{\partial t}\right)^T - \frac{2}{3}\nabla\cdot\frac{\partial \mathbf{u}_\mathrm{f}}{\partial t}\mathbf{I}\right) = \rho_\mathrm{f}\left(\frac{\partial^2 \mathbf{u}_\mathrm{f}}{\partial t^2}\right) \tag{4}$$

and

$$\frac{\partial p_\mathrm{f}}{\partial t} = -K_\mathrm{f}\nabla\cdot\left(\frac{\partial \mathbf{u}_\mathrm{f}}{\partial t}\right) \tag{5}$$

with the displacement vector $\mathbf{u}_\mathrm{f}$ and the bulk modulus K_f of the liquid. A more detailed derivation of equation (5) can be found in [3].

2.2. FE formulation and fluid-structure interaction

In a second step, the Finite-Element Method is employed to discretize the differential equations for the fluid. Based on the two-field incompressible elasticity (*u-p*) form [17], the implementation as a user-defined element in ANSYS (Version

www.czasopisma.pan.pl PAN POLSKA AKADEMIA NAUK www.journals.pan.pl

15.0) was carried out [2]. For the fluid, the resulting FE formulation then reads

$$\underbrace{\begin{bmatrix} \mathbf{M}^{\mathrm{f}}_{\mathrm{uu}} & \mathbf{0} \\ \mathbf{0} & \mathbf{0} \end{bmatrix}}_{\mathbf{M}^{\mathrm{f}}} \begin{bmatrix} \ddot{\mathbf{u}}^{\mathrm{f}} \\ \ddot{\mathbf{p}}^{\mathrm{f}} \end{bmatrix} + \underbrace{\begin{bmatrix} \mathbf{D}^{\mathrm{f}}_{\mathrm{uu}} & \mathbf{0} \\ \mathbf{0} & \mathbf{0} \end{bmatrix}}_{\mathbf{D}^{\mathrm{f}}} \begin{bmatrix} \dot{\mathbf{u}}^{\mathrm{f}} \\ \dot{\mathbf{p}}^{\mathrm{f}} \end{bmatrix} + \underbrace{\begin{bmatrix} \mathbf{0} & \mathbf{K}^{\mathrm{f}}_{\mathrm{up}} \\ \mathbf{K}^{\mathrm{f}}_{\mathrm{pu}} & \mathbf{K}^{\mathrm{f}}_{\mathrm{pp}} \end{bmatrix}}_{\mathbf{K}^{\mathrm{f}}} \begin{bmatrix} \mathbf{u}^{\mathrm{f}} \\ \mathbf{p}^{\mathrm{f}} \end{bmatrix} = \begin{bmatrix} \mathbf{F}^{\mathrm{f}} \\ \mathbf{0} \end{bmatrix} \tag{6}$$

with the nodal vector of the external fluid forces $\mathbf{F}^{\mathrm{f}}$, the symmetric mass matrix $\mathbf{M}^{\mathrm{f}}$, and damping matrix $\mathbf{D}^{\mathrm{f}}$. For the submatrices of the stiffness matrix $\mathbf{K}^{\mathrm{f}}$, which couple the nodal vectors of pressure $\mathbf{p}^{\mathrm{f}}$ and displacement $\mathbf{u}^{\mathrm{f}}$, $\mathbf{K}^{\mathrm{f}}_{\mathrm{up}} = \left(\mathbf{K}^{\mathrm{f}}_{\mathrm{pu}}\right)^T$ holds. Therefore, the stiffness matrix is symmetric, as well. However, this matrix is singular and thus no solution for the static state exists.

For the inner ear structures, a linear elastic behavior is assumed and an FE formulation based on displacement is state of the art. Since the motion of the fluid is described by displacements instead of velocities, the interaction with the structure is set up at the fluid-structure interface (FSI) by simply coupling the displacement degrees of freedom of the fluid with those of the structure

$$\mathbf{u}^{\mathrm{f}}|_{\mathrm{FSI}} = \mathbf{u}^{\mathrm{s}} \,. \tag{7}$$

This way, the previously appropriate partitioned matrices of the fluid and the structure are coupled and form a linear, second order system of differential equations

$$\mathbf{M}\ddot{\mathbf{q}} + \mathbf{D}\dot{\mathbf{q}} + \mathbf{K}\mathbf{q} = \mathbf{f} \tag{8}$$

with the symmetric mass $\mathbf{M}$, damping $\mathbf{D}$, stiffness $\mathbf{K}$ matrices and the nodal vectors of the generalized coordinates $\mathbf{q} = [\mathbf{u}^s, \mathbf{u}^f, \mathbf{p}^f]^T$ and the external forces $\mathbf{f} = [\mathbf{F}^s, \mathbf{F}^f, \mathbf{0}]^T$. In contrast to the commonly used partitioned approach, where the variable velocity is retained in the fluid equations, this monolithic approach allows one to solve the fluid-structure interaction problem without time-consuming integration and sub-iterations as well as without stability problems occurring in co-simulations. As the system of equations for the coupled problem is linear and the excitation of the cochlea is harmonic with the angular frequency Ω, the equation is formulated and solved in the frequency domain and reads

$$\left(-\Omega^2\mathbf{M} + j\Omega\mathbf{D} + \mathbf{K}\right)\tilde{\mathbf{q}} = \tilde{\mathbf{Q}} \tag{9}$$

with the imaginary unit j. The nodal vector $\tilde{\mathbf{Q}}$ contains the complex amplitudes of the excitation forces and $\tilde{\mathbf{q}}$ the complex amplitudes for the pressure and displacement.

3. Validation

In this section, the presented FE formulation for the fluid of the cochlea model is validated with a fluid-structure interaction. For this purpose, the frequency response of an oscillating beam vibrating in a viscous fluid is calculated and compared with the analytical solution.

www.czasopisma.pan.pl PAN POLSKA AKADEMIA NAUK www.journals.pan.pl

3.1. Oscillating beam in a viscous fluid

As shown in Fig. 1, the beam has a rectangular cross section and is immersed in a viscous fluid. Its left end is fixed at $z = 0$, whereas the unconstrained end is excited through the harmonic oscillating force $F_y(t) = F_y^* \exp(j\Omega t)$ with the angular frequency Ω. The dimensions and material properties for the beam and the fluid are given in Table 1 and are chosen according to the properties of the cochlea.

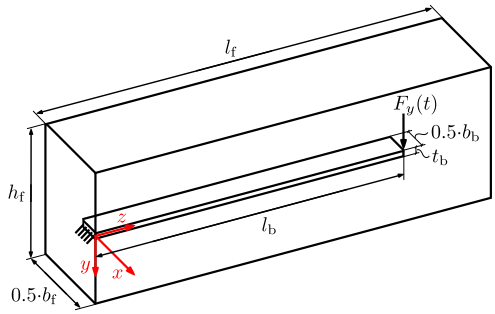

Fig. 1. System composed of an oscillating beam immersed in a viscous fluid used to validate the user-defined fluid element

Table 1.

Geometry and material properties for the beam and fluid

component	parameter	value
beam	length l_b	10 mm
	width b_b	1000 μm
	thickness t_b	100 μm
	density ρ_b	1000 kg/m^3
	Young's modulus E_b	$5{\cdot}10^9$ Pa
	Poisson ratio ν_b	0.3
fluid	length l_f	15 mm
	width b_f	4.5 mm
	height h_f	7 mm
	density ρ_f	1000 kg/m^3
	dynamic viscosity η_f	$1{\cdot}10^{-3}$ Pa·s
	bulk modulus K_f	$2{\cdot}10^9$ Pa

The material properties of the liquid are those of the cochlear fluid [13, 14]. In order to ensure that the boundary conditions of the fluid domain have no significant effect on the structural response, large dimensions of the fluid domain, compared to those of the beam, are used. Further, the material properties for the beam are in range with collagen fibers, which represent a basic component of biological membranes [8] and the geometry of the beam is in similar range with the dimensions of the basilar membrane.

The frequency response of the beam, which is effected by the inertial forces and viscous forces of the fluid, is calculated with a three dimensional FE-model. The beam is meshed with standard quadratic solid elements SOLID186. Ten elements were used along the thickness of the beam. For the liquid, the user-defined fluid element, Eq. (6), is used. At the wetted surfaces of the beam, the fluid-structure interaction is defined by the displacement constraint given by Eq. (7). In order to capture the viscous forces occurring in particular in the fluid close to the beam, this domain is discretized by fluid elements with an edge size of 3 µm. This yields 1300 solid elements and 90 000 fluid elements. The calculated frequency response for the unconstrained end of the beam at $z = l_\mathrm{b}$ is shown in Fig. 2.

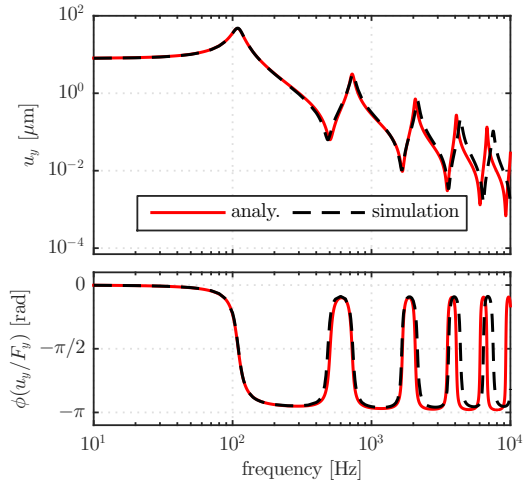

Fig. 2. Simulated frequency response and analytical solution for the unconstrained end of the beam vibrating in a viscous fluid

For the validation of the user-defined fluid element, the simulation results are compared with an analytical solution for the coupled system [18]. The derivation is based on the partial differential equation for the plane vibration of the beam in vacuum with its eigenfrequencies f_i. The loads acting on the beam are separated into the applied excitation force and the hydrodynamic load. For the latter one, the complex hydrodynamic function $\tilde{\Gamma}(\Omega)$ is introduced which depends on the oscillatory Reynolds number. Further, it is assumed that the mode shapes $M_i(\bar{z})$ of the beam in vacuum with the normalized coordinate $\bar{z} = z/l_\mathrm{b}$ remain valid for the coupled system as well. For small vibration amplitudes the displacement of the beam in y-direction is described by the analytical solution

$$\tilde{u}_y(\bar{z},\Omega) = \sum_{i=1}^{\infty} \frac{(\rho_\mathrm{b} A_\mathrm{b} l_\mathrm{b})^{-1} F_y^* M_i(\bar{z}=1) M_i(\bar{z})}{\left((2\pi f_i)^2 - \Omega^2 \left(1 + \dfrac{\pi {b_\mathrm{b}}^2 \rho_\mathrm{f} \tilde{\Gamma}(\Omega)}{4\rho_\mathrm{b} A_\mathrm{b}}\right)\right)} \tag{10}$$

www.czasopisma.pan.pl PAN POLSKA AKADEMIA NAUK www.journals.pan.pl

with the cross section A_b of the beam. This leads to the frequency response calculated for the right end of the beam at $z = l_b$, which is compared to the simulation results in Fig. 2.

Within the considered frequency range from 10 Hz to 10 kHz, the vibration amplitude of the beam shows several peaks. At these resonance frequencies, the phase, shown relative to the excitation force, changes by $\pm\,\pi$. Thereby, the change in phase is represented by a transition rather than a jump, and the resonance peaks in the amplitude curve are broad indicating damping effects. Since for the beam neither in the FE-model nor in the analytical solution structural damping is applied, the only source of damping is provided by the fluid, caused by viscous dissipation in the boundary layer.

In general, the simulation results for the frequency response of the beam are in good agreement with the analytical solution. For frequencies above 4 kHz, the results slightly differ. This discrepancy is due to spatial mode shapes of the beam occurring for higher excitation frequencies. While these spatial motions are captured in the three dimensional FE-model, the analytical solution is restricted to the plane vibration of the beam. Hence, these investigations confirm that, for small amplitudes, the user-defined fluid element is capable to accurately describe the dynamics of the fluid-structure coupled system. Therefore, this FE formulation will be used in the cochlea model to describe the fluid dynamics in the inner ear.

4. Cochlea model

In the following section, a passive FE-model of the human cochlea with simplified geometry is described. This passive model excludes consideration of amplification by electro-mobility of the outer hair cells. With this numerical model simulations are conducted investigating the fluid flow in the cochlea and the characteristic basilar membrane vibration leading to hearing sensation. The dimensions and material properties for the fluid and cochlear structures are presented with particular focus on the basilar membrane. This membrane is treated as passive. That means, the cochlear amplifier within the organ of Corti containing the active outer hair cells, is not represented in this model. Additionally, the excitation through the oscillatory motion of the stapes footplate and the evaluation of the results are specified.

4.1. Fluid spaces and cochlear structures

The geometry of the FE-model is shown in Fig. 3. In contrast to the anatomy of the inner ear, the fluid-filled chambers are uncoiled. This simplification regarding the geometry is commonly accepted in the field of inner ear mechanics [19, 20], since the coiling of the fluid spaces is assumed to have only a minor effect on cochlear dynamics [21]. The lower chamber, scala tympani, is separated from the upper chamber, scala vestibuli by the basilar membrane, which is embedded by the

www.czasopisma.pan.pl PAN POLSKA AKADEMIA NAUK www.journals.pan.pl

spiral ligament and spiral lamina to a bony wall. At the basal end, scala vestibuli is connected to the vestibulum, a fluid-filled cavity which comprises the stapes footplate. At the apex, both chambers are connected by the helicotrema. Since the compliant round window membrane at the basal end of the scala tympani prevents any leakage of inner ear fluid, and neglecting the cochlear aqueduct, the cochlea can be considered as a closed hydraulic system.

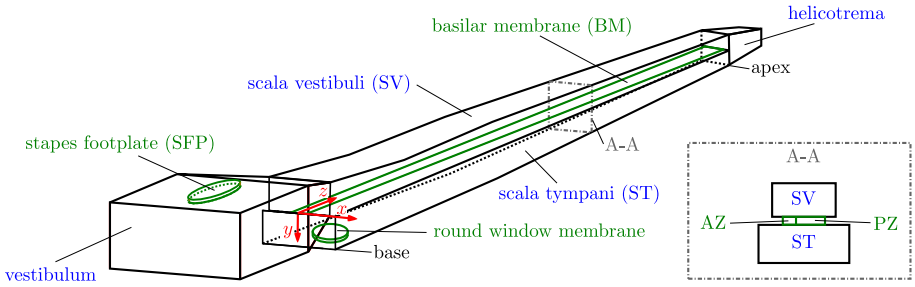

Fig. 3. Geometry of the human cochlea model

Because the basilar membrane is much more compliant than the bony wall, as well as the spiral lamina and spiral ligament, all three structures are approximated as rigid. The fluid domain has a total length of 41 mm and adds up to a volume of 110 mm^3. The distribution of the fluid volume along the cochlea model is based on anatomical data for the human cochlea [22, 23] assuming a rectangular cross section for the conical chambers. For the discretization of the liquid, 350 000 hexahedral user-defined fluid elements, Eq. (6), are used. In order to capture the dynamic effects within the fluid boundary layers, fluid elements in these zones of the model have an edge size of 2 μm. In the FE-model, boundary conditions are applied to the fluid domain to represent the rigid walls of the cochlear chambers. For this, the three displacement degrees of freedom of the corresponding fluid nodes are constrained to zero. The material properties of the inner ear liquid are similar to those of a salt-water solution [13, 14]. Therefore, the density, dynamic viscosity and bulk modulus for water are used, Table 1.

The stapes footplate is hosted in the upper wall of the vestibulum. It has an oval shape with an area of 3.1 mm^2. Its material behavior is assumed to be linear elastic and for the bone the Young's modulus of 14100 MPa, the density of 2200 kg/m^3 and the Poisson ratio of 0.3 are used [24, 25]. The compliant round window membrane, located in the lateral basal wall of the scala tympani, is modeled as a cylindrical membrane with clamped edges. Its geometry with an area of 2.1 mm^2 and a thickness of 70 μm is based on anatomical data [26, 27]. Due to experimental results [28], small vibration amplitudes of the membrane are expected and a linear elastic material description is used with a Poisson ratio of 0.3, a density of 1200 kg/m^3 and a Young's modulus of 40 kPa which is in range with the apical Young's modulus of the basilar membrane [29]. Preliminary numerical investigations not presented in this work, in which the Young's modulus was varied

www.czasopisma.pan.pl PAN POLSKA AKADEMIA NAUK www.journals.pan.pl

in morphologically reasonable boundaries, have shown that the basilar motion is only very little affected by the particular value of Young's modulus. Hence, the use of a simple linear elastic material without frequency dependence is considered appropriate.

Both the stapes footplate and round window membrane are meshed with quadratic solid elements SOLID186. To define the fluid-structure interaction, the displacement degrees of freedom of the nodes on the wetted surfaces of the round window membrane and the stapes footplate are coupled with those of the fluid, Eq. (7).

4.2. Basilar membrane

The basilar membrane, as an elastic partition, separates the two fluid-filled chambers and has a length L_{Bm} of 31 mm [30]. The width of the tapered membrane increases in the FE-model exponentially from 80 μm at the base to 500 μm at the apex. However, its thickness decreases linearly from 34 μm to 12 μm towards the helicotrema. While for the estimation of the basilar membrane width μ-CT data are used [31], these data are not appropriate to determine the membrane's thickness due to the limited resolution. Therefore, anatomical data for humans [32, 33] are used instead, and are in range with the thickness distribution in cats [34].

From a morphologic point of view [7–9] the basilar membrane can be divided in cross section into two distinct zones, the arcuate zone and the pectinate zone, Fig. 4. In the arcuate zone, the filaments show relatively low stiffness, are evenly distributed and embedded in a gelatinous ground substance [35]. In contrast, the filaments in the pectinate zone are grouped into fibers, which in turn are organized into transversally orientated bands and are immersed in a gelatinous ground substance [9, 34, 36]. Therefore, in this model, an orthotropic material description is used for the pectinate zone. This orthotropic material has isotropic material properties along the t- and r-axes but has different material properties along the s-axis. Although this material is called transversal-isotropic or polar-anisotropic in some references, in this work, the general term orthotropic is used. For the arcuate zone, an isotropic material behavior is assumed. This model is further motivated by the experimental findings in [35]. Even though in [35] only basilar membranes of gerbils were investigated, those findings are adopted for the human case because the authors were unable to find morphological data for the human arcuate zone in current literature. There are, certainly, differences between the basilar membrane of gerbils and humans, however, they are assumed to be sufficiently small. Thereby, the ratio between the pectinate and arcuate zone in width is 1:2, according to anatomical data [34, 37]. The AZ and PZ are kinematically coupled by eliminating redundant degrees of freedom of overlapping nodes. This two-zone modelling approach for the human basilar membrane is based on first approaches published in [38, 39] and colorredis in contrast to most other FE-models of the basilar membrane, which ignore the morphologic differences of these zones assuming an isotropic material behavior

www.czasopisma.pan.pl PAN POLSKA AKADEMIA NAUK www.journals.pan.pl

for the entire membrane, e.g. [5, 6]. The coordinate system shown in Fig. 4 has its origin at the basal junction between the AZ and PZ in the middle of the basilar thickness. The s-axis points along the junction in apical direction and the r-axis points away from the AZ.

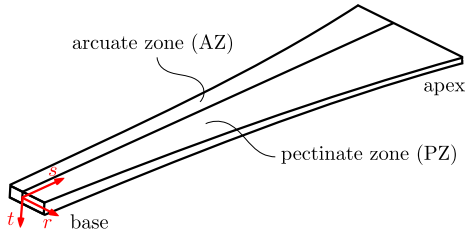

Fig. 4. Model of the basilar membrane composed of two zones taking different morphologic structures into account

The orthotropic material description reads

$$\epsilon = \mathbf{C}^{\mathrm{PZ}}\sigma \tag{11}$$

which contains the compliance matrix

$$C^{\mathrm{PZ}} = \begin{bmatrix} \frac{1}{E_r^{\mathrm{PZ}}} & -\frac{\nu_{rs}^{\mathrm{PZ}}}{E_r^{\mathrm{PZ}}} & -\frac{\nu_{rs}^{\mathrm{PZ}}}{E_r^{\mathrm{PZ}}} & 0 & 0 & 0 \\ -\frac{\nu_{rs}^{\mathrm{PZ}}}{E_r^{\mathrm{PZ}}} & \frac{1}{E_t^{\mathrm{PZ}}} & -\frac{\nu_{st}^{\mathrm{PZ}}}{E_s^{\mathrm{PZ}}} & 0 & 0 & 0 \\ -\frac{\nu_{rs}^{\mathrm{PZ}}}{E_r^{\mathrm{PZ}}} & -\frac{\nu_{st}^{\mathrm{PZ}}}{E_s^{\mathrm{PZ}}} & \frac{1}{E_s^{\mathrm{PZ}}} & 0 & 0 & 0 \\ 0 & 0 & 0 & G_1 & 0 & 0 \\ 0 & 0 & 0 & 0 & G_2 & 0 \\ 0 & 0 & 0 & 0 & 0 & G_2 \end{bmatrix} \tag{12}$$

with the coefficients

$$G_1 = \frac{1+\nu_{st}^{\mathrm{PZ}}}{0.5E_s^{\mathrm{PZ}}}, \qquad G_2 = \frac{1}{G_{rs}^{\mathrm{PZ}}} \tag{13}$$

as well as the vector for the strains $\epsilon = [\epsilon_{rr} \quad \epsilon_{tt} \quad \epsilon_{ss} \quad 2\epsilon_{ts} \quad 2\epsilon_{sr} \quad 2\epsilon_{rt}]^T$ and the vector for the stresses $\sigma = [\sigma_{rr} \quad \sigma_{tt} \quad \sigma_{ss} \quad \tau_{ts} \quad \tau_{sr} \quad \tau_{rt}]^T$. Thus, five material parameters have to be defined for the pectinate zone, whereas for the isotropic arcuate zone, two material parameters, the bulk modulus K^{AZ} and the Young's modulus E^{AZ} are sufficient to define the material formulation [40]. In the following, these material properties are defined based on data published in literature.

The basilar membrane behaves isotropic in both zones at the apex [41, 42]. This seems reasonable for the pectinate zone as well, since the volume fraction of

fiber bands in the apical pectinate zone is reported to be quite low compared to the ground substance [42, 43]. Therefore, it is expected that the Young's modulus of the ground substance E_{GS} dominates the Young's moduli of both zones at the apex $s = L_{\mathrm{BM}}$. Choosing $E_{GS} = 40$ kPa, which is in range with experimental findings [42, 43], it follows

$$E^{\mathrm{AZ}} = E_t^{\mathrm{PZ}} = E_s^{\mathrm{PZ}} = E_r^{\mathrm{PZ}}(s = L_{\mathrm{BM}}) = E_{GS}. \tag{14}$$

As shown by experiments, the stiffness of the pectinate zone is dominated by the radially-orientated bands [35, 41–43]. Further, measurements indicate an exponentially increasing diameter of these bands from the apex towards the base [44]. Therefore, the radial Young's modulus of the pectinate zone is assumed to increase exponentially towards the base

$$E_r^{\mathrm{PZ}}(s) = E_r^{\mathrm{PZ}}(s = 0)e^{c_1 s} \tag{15}$$

with

$$c_1 = \ln\left(\frac{E_r^{\mathrm{PZ}}(s = L_{\mathrm{BM}})}{E_r^{\mathrm{PZ}}(s = 0)}\right) {L_{\mathrm{BM}}}^{-1}. \tag{16}$$

Assuming an increase from the apex towards the base by 10-fold, which seems to be in a reasonable range [42], the radial Young's modulus at the base for the pectinate zone is $E_r^{\mathrm{PZ}}(s = 0) = 300$ kPa. In contrast, the transversal Young's moduli E_s^{PZ} and E_t^{PZ} stay constant in space.

Although the stiffness in the pectinate zone is dominated by the radially-orientated bands, the volume fraction of the fibers compared to the ground substance does not exceed 20 % in the basal domain [42]. Further, the ground substance is described as an incompressible, gelatinous material [43, 45]. Therefore, it is assumed that the bulk modulus of the basilar membrane is equal to the bulk modulus of the cochlear fluid K_{f}. This completes the material description for the arcuate zone

$$K^{\mathrm{AZ}} = K_{\mathrm{f}}. \tag{17}$$

The effective bulk modulus for the pectinate zone $K_{\mathrm{eff}}^{\mathrm{PZ}}$ then reads

$$K_{\mathrm{eff}}^{\mathrm{PZ}} = K_{\mathrm{f}} \tag{18}$$

and leads to the Poisson ratios

$$\nu_{rs}^{\mathrm{PZ}} = 0.5 - \frac{E_r^{\mathrm{PZ}}}{6K_{\mathrm{f}}} \tag{19}$$

and

$$\nu_{st}^{\mathrm{PZ}} = 1 - \frac{E_s^{\mathrm{PZ}}(E_r^{\mathrm{PZ}} + 3K_{\mathrm{f}})}{6E_r^{\mathrm{PZ}}K_{\mathrm{f}}}. \tag{20}$$

To complete the material description for the pectinate zone, the shear modulus G_{rs}^{PZ} is defined. Since no experimental data are available for the shear modulus, an isotropic approach is assumed leading to

$$G_{rs}^{\mathrm{PZ}} = \frac{E_r^{\mathrm{PZ}}}{2(1+\nu_{rs}^{\mathrm{PZ}})}. \tag{21}$$

For both zones of the basilar membrane, a density of $\rho^{\mathrm{AZ}} = \rho^{\mathrm{PZ}} = 1200$ kg/m^3 is used and is in range with that for the tympanic membrane and round window membrane [29, 46]. The damping matrix for the basilar membrane is defined proportional to the stiffness matrix and for both zones a spatial constant factor of $\xi_{BM} = 0.07$ is used and seems reasonable [39]. This is in contrast to the approach described in [5, 47]. There, an arbitrary spatial distribution of Rayleigh damping coefficients along the basilar membrane is required probably caused by treating the entire basilar membrane as an isotropic material contradicting the real anatomic structure of the membrane.

In the FE-model, the basilar membrane is meshed by 12 000 quadratic SOLID186 elements. Five elements were used along the thickness of the beam. The edges of the membrane are clamped and the displacement degrees of freedom of the nodes on the wetted surfaces of the membrane are coupled with those of the fluid, Eq. (7). The most important geometry and material properties for the fluid and the basilar membrane are summarized in Table 2. Further details of the FE-model are described in the following work [48].

Table 2.
Most important geometry and material properties for the developed FE-model of the human cochlea

component	parameter	value
fluid	volume V_{f}	110 mm^3
	density ρ_{f}	1000 kg/m^3
	dynamiv viscosity η_{f}	$1{\cdot}10^{-3}$ Pa·s
	bulk modulus K_{f}	$2{\cdot}10^9$ Pa
basilar membrane	length l_{BM}	31 mm
	width b_{BM}	80 µm...500 µm
	thickness t_{BM}	34 µm...12 µm
	density $\rho^{\mathrm{AZ}} = \rho^{\mathrm{PZ}}$	1200 kg/m^3
basilar membrane AZ	Young's modulus E^{AZ}	40 kPa
	bulk modulus K^{AZ}	$2{\cdot}10^9$ Pa
basilar membrane PZ	Young's modulus E^{PZ}	see Eq. (14-16)
	Poisson ratio ν_{rs}^{PZ}	see Eq. (19)
	Poisson ratio ν_{st}^{PZ}	see Eq. (20)
	shear modulus G_{rs}^{PZ}	see Eq. (21)

www.czasopisma.pan.pl PAN POLSKA AKADEMIA NAUK www.journals.pan.pl

4.3. Excitation and evaluation of results

The FE-model of the human cochlea is excited by the harmonic oscillation of the stapes footplate. The excitation of the stapes footplate may consist of translational and rotational motion, as shown in [49]. Here, only translational, i.e. piston-like excitation is considered and presented. Results for rotational excitation can be found in [48]. The physiological amplitudes of the stapes footplate measured for an ear canal sound pressure of 80 dB_{SPL} in human temporal bone specimens [49] are applied as kinematic constraints to the FE-model. The entire model sums up to about 370 000 elements and the linear set of equations, see Eq. 9, is then solved in the frequency domain within around 5 hours for each frequency. For the simulation results shown in the following, the motion of the basilar membrane, the fluid pressure, and velocities are evaluated at $x = 0$ in the vertical median yz plane of the cochlea model.

5. Results

In this section, first the simulation results for the basilar membrane vibration, the fluid velocities and pressure are shown for one single excitation frequency. Then, the dynamic behavior of the cochlea model for different excitation frequencies within the human audible frequency range is investigated.

5.1. Basilar membrane vibration

Hearing nerve stimulation results from the vibration of the basilar membrane leading to shearing of the hair cells which are placed on the basilar membrane. For a deeper understanding of the formation of hearing sensation, therefore, the characteristic vibration behavior of the basilar membrane is of central interest. In Fig. 5, the transversal vibration amplitude and phase of the basilar membrane are shown relative to the amplitude of the stapes footplate along the s-axis of the basilar membrane length for an excitation frequency of 2 kHz.

At the base, the amplitude of the basilar membrane is quite small and is in the order of a few nanometers. Towards the apex, the amplitude increases reaching a maximum amplitude of 125 nm at the characteristic longitudinal position $z = 15.5$ mm. Beyond that point, the amplitude decreases rapidly. Thus, the vibration is totally ceased around $z = 25$ mm and results in an asymmetric amplitude response. At the base, the phase of the basilar membrane vibration leads that of the stapes footplate by $+\pi/2$. Towards the apex, at first, the phase decreases slightly, then, around the characteristic position, it decreases strongly and eventually reaches a plateau value of around -40π just beyond that point. Apical to $z = 25$ mm, the phase can no longer be interpreted, since in this domain the vibration amplitude of the basilar membrane is numerically zero.

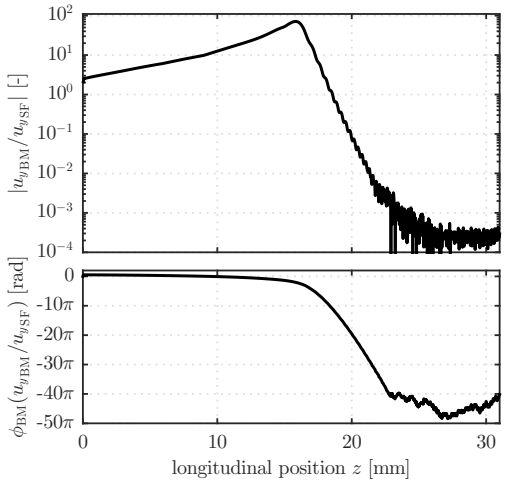

Fig. 5. Amplitude and phase of the basilar membrane relative to that of the stapes footplate shown along the cochlea model for 2 kHz

The decrease in phase with the longitudinal position represents the formation of a wave on the basilar membrane. This wave becomes apparent in Fig. 6, which shows the instantaneous amplitude of the basilar membrane vibration for three different points of time of a cycle as well as the corresponding envelopes.

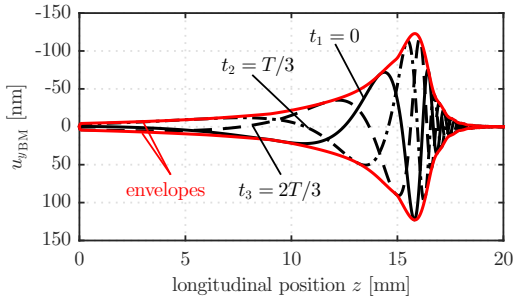

Fig. 6. Instantaneous amplitude of the basilar membrane and corresponding envelopes shown along the cochlea model for 2 kHz

The peak of this wave travels from the base towards the apex, while the amplitude of this wave increases. At the characteristic position, the so-called traveling wave reaches its maximum amplitude. Mainly in this local domain, the stereocilia of the inner hair cells placed on the basilar membrane get sheared and result in hearing nerve stimulation. Beyond the characteristic position, the amplitude of the traveling wave declines rapidly. However, just before the vibration amplitude totally ceases, the traveling wave changes into a standing wave, indicated by the phase plateau in Fig. 5. As further simulations in [48] show, for higher excitation frequencies this phase plateau occurs closer to the base. At the same time, the

www.czasopisma.pan.pl PAN POLSKA AKADEMIA NAUK www.journals.pan.pl

level of the phase plateau is shifted to smaller phase values. This separates it more clearly from the numerical noise level and the phase plateau becomes even more pronounced. Along with experimental investigations [50], this is a clear evidence for the existence of a standing wave in the cochlea, which occurs for higher frequencies well beyond the characteristic position. The developed FE-model is capable of describing this behavior and further numerical investigations will be conducted in order to understand the formation of standing waves in the cochlea as well as to clarify to what extend these waves of small amplitude may contribute to hearing sensation.

The simulation results for the FE-model of the human cochlea show the formation of a traveling wave on the basilar membrane. This is in agreement with the observations during experiments on human temporal bone specimen [51]. Since for these investigations the fluid chambers were opened and unphysiological high ear canal sound pressures above 140 dB_{SPL} were used, a quantitative comparison with the simulation results is not possible. Further, recent measurements of the basal basilar membrane vibration in gerbils [52] confirm the formation of a traveling wave in the mammalian cochlea.

In literature, only very few measurements of the basilar membrane vibration in human temporal bone specimen exist. In addition, these measurements are conducted only in a few number of single points along the membrane. Therefore, the simulated basilar membrane vibration cannot be validated quantitatively along its entire length, but only in these very few points. In the following, the simulated amplitude of the basilar membrane is validated locally at $z = 12$ mm by use of the measurement in a human temporal bone [53]. The locally measured amplitude ratio of the basilar membrane to the stapes footplate for 2 kHz is around 25 dB. Since the amplitude ratio for the FE-model with 26 dB is in similar range, Fig. 5, the simulation results for the basilar membrane vibration amplitude are likely to be reasonable. However, since in [53] measurements are only available for one single location, the simulation results can only be compared for this location. It should be emphasized at this point that the orthotropic material formulation of the basilar membrane presented here is based on its morphologic structure. Further, realistic material parameters from experimental studies are used, which can be assigned to the components of the membrane. This is in contrast to many other FE-models, e.g., [6]. There, often a purely isotropic material description is used, and usually material parameters are fitted with respect to tonotopy. However, this is in contradiction to the morphologic structure of the basilar membrane's pectinate zone with its radially-orientated bands and results in questionably high Young's moduli. The fundamental behavior of the phase shift also fits quite well compared with these measurements in human temporal bones [53]. Altogether, the presented two-zone material description for the basilar membrane seems appropriate to describe its characteristic vibration pattern. However, the absolute value of the phase shift with around 20 cycles is quite high, especially compared with other FE-models, [54]. These high values may be caused by neglecting the additional mass of the organ of

Corti or by the influence of neglected fluid damping on the phase shift in this passive cochlea model. Both assumptions are of concern for further detailed studies.

In the following, two characteristic properties of the traveling wave are discussed, i.e., the wavelength and the phase velocity. In Fig. 6, it can be seen that the wavelength at the base of the basilar membrane is around 110 mm and thus is large compared to the dimensions of the cochlea. Towards the apex, the wavelength decreases strongly and is around 1 mm close to the characteristic position. This indicates that the velocity of the wave alters along the length of the membrane. Therefore, the wave velocity $v_{\phi\mathrm{BM}}$ is calculated for the traveling wave

$$v_{\phi\mathrm{BM}}(z) = 2\pi f \left| \left(\frac{d\phi_{\mathrm{BM}}(z)}{dz} \right)^{-1} \right| \tag{22}$$

with the constant frequency $f = 2$ kHz and the local phase gradient $d\phi_{\mathrm{BM}}/dz$, calculated from Fig. 5. As shown in Fig. 7, the velocity of the traveling wave has its maximum of about 220 m/s at the base. Due to the shortening of the wave length towards the apex, the propagation of the traveling wave gets increasingly delayed. Therefore, the wave velocity decreases strongly along the length of the membrane towards the apex and is in the range of 1 m/s close to the characteristic position.

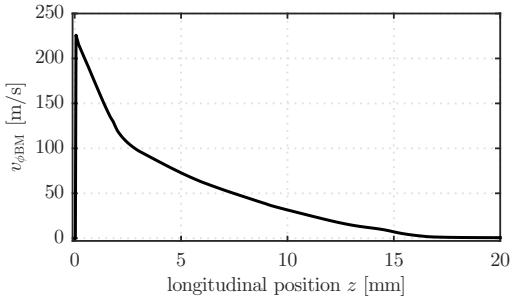

Fig. 7. Phase velocity of the traveling wave along the basilar membrane at 2 kHz

For comparison, the velocity of the pressure waves in the inner ear fluid is calculated by the use of the fluid properties given in Table 1

$$c_{\mathrm{f}} = \sqrt{K_{\mathrm{f}}/\rho_{\mathrm{f}}} = 1414 \text{ m/s}. \tag{23}$$

Thus, the velocity of the traveling wave on the basilar membrane at the base is around one order lower and even more than two orders of magnitude lower close to the characteristic position as compared to the velocity of the pressure waves in the cochlear fluid. This clearly demonstrates two different time scales in the cochlea. There is a fast time scale represented by the fast pressure waves and a slower time scale represented by the traveling wave on the basilar membrane. This illustrates that the traveling wave is not a direct result of the traveling pressure

waves. Instead, the slower scale only becomes evident by investigating the fluid velocity field and the related fluid-structure interaction in the cochlea model. This interaction is further discussed in the following.

5.2. Fluid velocity

The investigation of the fluid velocity distribution and derived velocity profiles provide novel insights into the cochlear flow and enables us to classify the fluid flow. Further, the simulations allow us to identify the viscous damping mechanism which is responsible for the formation of the traveling wave. Additionally, the results provide a first indication regarding the impact of coiling of the fluid chambers on the apical fluid flow.

In Fig. 8, the instantaneous longitudinal fluid velocity field in the vertical median plane of the FE-model can be seen for an excitation frequency of $f = 2$ kHz. Additionally, the instantaneous transversal basilar membrane and the stapes footplate amplitude are shown, scaled by 2500 and 75 000-fold, respectively.

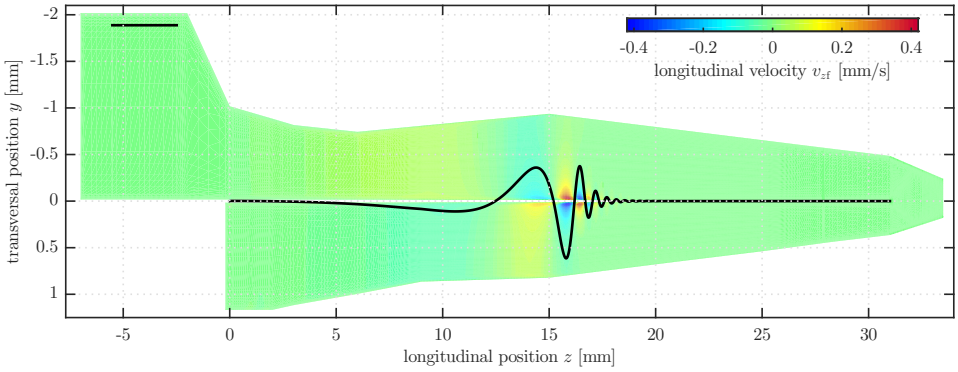

Fig. 8. Instantaneous longitudinal fluid velocity field and basilar membrane vibration shown in the vertical median plane of the FE-model for an excitation frequency of 2 kHz

In the entire fluid domain, the longitudinal fluid velocity is quite low. The maximum longitudinal velocity v_{zf} with around 0.4 mm/s occurs in the fluid layer close to the basilar membrane near to the characteristic position at $z = 15.5$ mm. With a characteristic length of $L = 500$ µm, which is in range of the width of the basilar membrane, the fluid viscosity η_f and density ρ_f from Table 1, the maximum Reynolds number is

$$\mathrm{Re} = \frac{\rho_f L v_{zf}}{\eta_f} = 0.2. \tag{24}$$

Since this dimensionless number is well below one for the entire fluid domain, the fluid flow in the cochlea can be regarded as a creeping flow. The Womersley

www.czasopisma.pan.pl PAN POLSKA AKADEMIA NAUK www.journals.pan.pl

number, characterizing the unsteadiness of the fluid flow in the cochlear system, is

$$\mathrm{Wo} = L\sqrt{\frac{2\pi f \rho_\mathrm{f}}{\eta_\mathrm{f}}} = 56. \tag{25}$$

In contrast to the Reynolds number, the Womersley number is well above one. This indicates that the fluid flow in large sections of the fluid domain is dominated by the unsteady inertia forces of the fluid, rather than the viscous forces.

The consequences for the resulting fluid velocity profile can be clearly seen in Fig. 9. There, the instantaneous distribution of the longitudinal fluid velocity along the cross section of the scala vestibuli and scala tympani is shown for the basal domain. The times t_1 to t_4 in Fig. 9 are chosen such that t_1 is at 0°, t_2 at 30°, t_3 at 60° and t_4 at 90° with respect to the harmonic stapes footplate excitation. Since in the basal region, the basilar membrane amplitude is still quite small, the membrane can be regarded for simplicity as a rigid wall. Therefore, the velocity profile is almost symmetric to the center of the cross section. As t_1 through t_4, capture the first quarter cycle of the stapes footplate, the majority of velocities are negative. The velocity profile characteristics are similar to the velocity profile for an unsteady flow through a rigid pipe [55]. The prominent plateau, evoked by the unsteady inertia forces, extends from the center towards the boundaries of the cross section. Except of the fluid layers close to the rigid wall and the basilar membrane, the velocity profile alters significantly. In these fluid layers, the viscous forces dominate compared to the unsteady inertia forces. Due to the no-slip boundary condition applied to the fluid in order to represent the rigid walls of the fluid chambers and the displacement constraints at the fluid-structure interface at the basilar membrane, the longitudinal fluid velocities there are zero or almost zero,

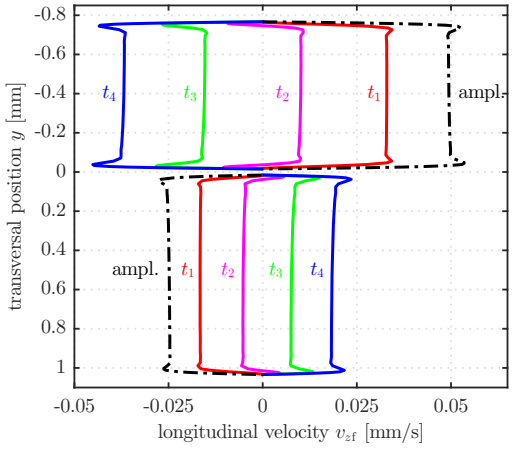

Fig. 9. Instantaneous distribution of the longitudinal fluid velocity along the cross section of scala vestibuli and scala tympani at the base $z = 5$ mm

www.czasopisma.pan.pl PAN POLSKA AKADEMIA NAUK www.journals.pan.pl

respectively. This results in substantial velocity gradients in these so-called viscous boundary layers.

However, in the cross section of the chambers close to the characteristic position, where the basilar membrane amplitude exhibits its maximum, the velocity profile changes considerably, Fig. 10. Whereas the longitudinal fluid velocity close to the rigid wall of the chambers hardly alters, the velocity in the viscous boundary layer close to the basilar membrane increases significantly. This results in an asymmetric velocity profile characterized by significantly increased velocity gradients in the fluid layer close to the basilar membrane. These velocity gradients in turn lead to viscous damping forces acting on the basilar membrane due to the fluid-structure interaction. In this way, the vibration amplitude of the membrane decreases rapidly beyond the characteristic position resulting in a global maximum along the cochlea, Fig. 6. Further, these viscous damping forces cause an increasing phase delay of the basilar membrane vibration which eventually results in the traveling wave caused by the mechanisms explained in the previous section.

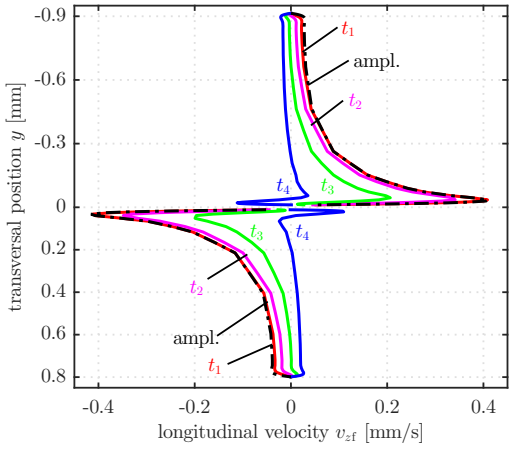

Fig. 10. Instantaneous distribution of the longitudinal fluid velocity along the cross section of scala vestibuli and scala tympani close to the characteristic position z = 15.5 mm

The results show clearly that although the viscosity of the cochlear fluid, which is in the range of water, may at a first glance seem negligibly low, the viscous forces significantly affect the fluid flow and the resulting basilar membrane vibration. Therefore, these forces have to be taken into account in order to simulate the cochlear dynamics. As further investigations showed, for lower values of fluid viscosity the basilar membrane vibration does no longer totally decay before reaching the apex [48]. In particular for lower excitation frequencies, this in turn leads to reflections in the apical region of the cochlea which contradicts with the spatial frequency mapping of the hearing organ. The user-defined fluid element employed in this study is capable of completely describing the viscous creeping flow in

www.czasopisma.pan.pl PAN POLSKA AKADEMIA NAUK www.journals.pan.pl

the human inner ear and provides an approach to compute the basilar membrane vibration pattern resulting from the fluid-structure interactions in an efficient way.

In contrast, standard acoustic elements neglect the viscous damping forces generated in the fluid boundary layers. Even though, these elements are rarely used in FE-models of the cochlea in order to try to calculate the cochlear fluid flow and the resulting basilar membrane vibrations [4]. Then, arbitrarily-defined impedance surfaces in the fluid domain or spatial distributions of structural damping coefficients for the basilar membrane are applied in order to introduce sufficient damping to the cochlea model. However, this approach can be regarded as a numerical approximation of the resulting basilar membrane vibration pattern, rather than physical modeling. Further, the use of acoustic elements leads to a constant fluid velocity profile in the cross-section of the chambers. Therefore, these elements are not appropriate to describe accurately the cochlear fluid and structural dynamics.

Beyond the characteristic position, the amplitude of the basilar membrane vibration decreases rapidly and is totally ceased in the apical domain. Therefore, the fluid velocity profile in this domain, Fig. 11, has a similar characteristic as the velocity distribution in the basal domain, Fig. 9. However, the amplitude of the longitudinal fluid velocity at the apex is about three orders lower compared to the base. The significant deformation of the basilar membrane at the characteristic position leads, in particular in this domain, to the interaction between the fluid in the scala vestibuli and scala tympani. Thus, mainly in this domain the fluid flow is already diverted into the scala tympani, rather than at the helicotrema. This is a further possible reason, why the coiling of the cochlear fluid chambers plays a minor role for the cochlear fluid flow and the resulting vibration pattern of the basilar membrane. This justifies the geometry of the FE-model presented in section 4.1 in retrospect.

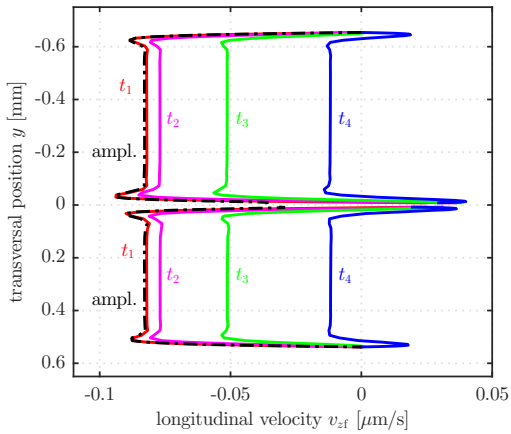

Fig. 11. Instantaneous distribution of the longitudinal fluid velocity along the cross section of scala vestibuli and scala tympani at the apex $z = 25$ mm

5.3. Fluid pressure

In the following, the fluid pressure distribution in the cochlear fluid is discussed in order to explain the excitation of the characteristic basilar membrane vibration. Thereby, the significance of the round window membrane as well as of the inertia and the compressibility of the fluid for the resulting pressure difference which in turn evokes the traveling wave is clarified.

At first, the calculated fluid pressure distribution in the cochlea model is discussed for an excitation frequency of 2 kHz. In Fig. 12, the instantaneous pressure field in the vertical median plane of the FE-model can be seen. For this time point, the stapes footplate is moving out of the vestibulum and the amplitudes of the basilar membrane and the stapes footplate are shown scaled by 2500 and 75 000-fold respectively.

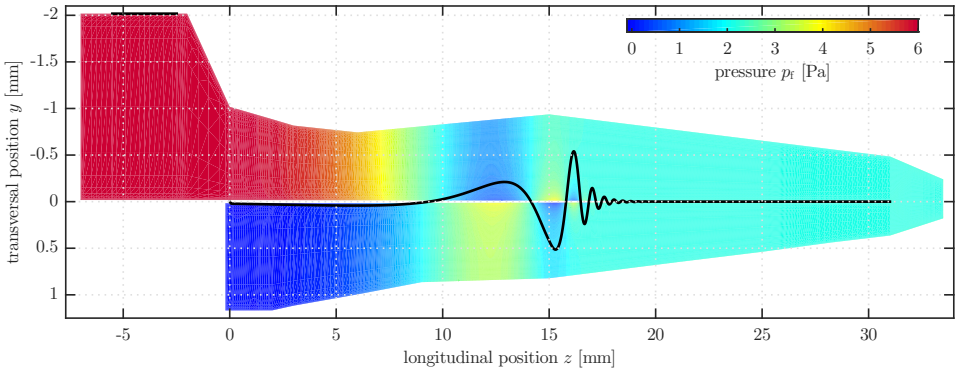

Fig. 12. Instantaneous fluid pressure field and basilar membrane vibration shown in the vertical median plane of the FE-model for an excitation frequency of 2 kHz

The simulation results show that the maximum amplitude of the fluid pressure in the cochlea is around 6 Pa and, therefore, quite low compared to classical engineering flow problems. This maximum fluid pressure occurs in the vestibulum close to the stapes footplate. Comparing the fluid pressure in the vestibulum with the sound pressure of 80 dB_{SPL} = 0.2 Pa in the ear canal, this demonstrates clearly a pressure amplification between the outer and inner ear. This gain is provided by the middle ear, since the area of the tympanic membrane is much larger compared to that of the stapes footplate. Additionally, the lever action of the middle ear bones results in a further amplification of the pressure.

From the vestibulum and the basal domain of the scala vestibuli, the fluid pressure decreases towards the apex. This is in contrast to the fluid pressure in the scala tympani, where the pressure amplitude is lowest in the basal domain and increases towards the characteristic position. Since the round window membrane, located in the lateral basal wall of the scala tympani, is very compliant, this structure offers no significant resistance against the displacement of the fluid in this domain. This

www.czasopisma.pan.pl PAN POLSKA AKADEMIA NAUK www.journals.pan.pl

results in an pressure amplitude of almost 0 Pa at the basal end of the scala tympani. Therefore, the simulation results indicate that the round window membrane can be regarded as a closure of the scala tympani with negligible stiffness mainly preventing the cochlear fluid from leakage. Apical to the characteristic position, the fluid pressure in both chambers has an equal amplitude and oscillates in phase. In particular, within the fluid close to the basilar membrane and the characteristic position, the instantaneous fluid pressure field in Fig. 12 indicates significant pressure gradients in the direction normal to the basilar membrane. As further evaluations showed [48], thereby the pressure amplitude decreases with increasing distance from the basilar membrane, which is in accordance with experimental findings [56].

The pressure distribution in the fluid-filled chambers results in a pressure difference across the basilar membrane. For the instantaneous pressure field, Fig. 12, the resulting pressure difference between scala vestibuli and scala tympani is shown in Fig. 13 as well as its amplitude. This pressure difference evokes the characteristic basilar membrane vibration. Its amplitude with about 6 Pa is maximal at the base of the cochlea model. With increasing vibration amplitude of the basilar membrane towards the apex, Fig. 6, the amplitude of the pressure difference across the membrane decreases. At the characteristic position, the large vibration amplitude of the basilar membrane leads in this domain to an interaction between the fluid flow in the scala vestibuli and scala tympani. Thus, the pressure difference across the basilar membrane is already compensated in this sector of the fluid domain, rather than at the helicotrema.

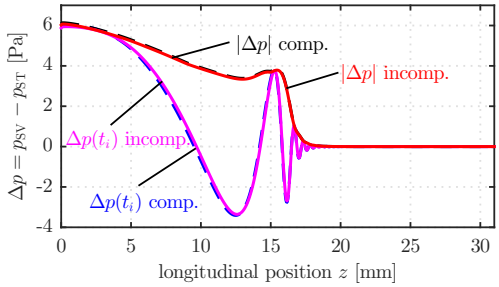

Fig. 13. Fluid pressure difference between scala vestibuli and scala tympani for the slightly compressible and incompressible cochlear fluid shown along the cochlea model at 2 kHz

The pressure difference between the fluid-filled scala vestibuli and scala tympani is responsible for the excitation of the basilar membrane, which in turn results in hearing nerve stimulation. In order to develop a deeper understanding for the excitation of the traveling wave on the basilar membrane and thus for the generated hearing sensation, the formation of this pressure difference is investigated.

The cochlear fluid is slightly compressible. This may suggest that along the fluid chambers a standing pressure wave resulting from the compressibility of

www.czasopisma.pan.pl PAN POLSKA AKADEMIA NAUK www.journals.pan.pl

the fluid is developed. This standing pressure wave then may cause a pressure difference across the scala vestibuli and scala tympani, which in turn may evoke the characteristic vibration pattern of the basilar membrane. If the pressure difference primarily results from the compression of the cochlear fluid, the calculated pressure difference must alter considerably with an increase of the bulk modulus of the fluid. However, this is not the case, as shown in Fig. 13. Although the bulk modulus of the cochlear liquid is increased by several orders and thus the fluid for this case can be regarded as incompressible, the pressure difference across the basilar membrane hardly changes.

This finding can be explained, if the wave length λ_f of the standing pressure wave in the slightly compressible fluid is compared to the dimensions of the fluid chambers. For an excitation frequency of $f = 2$ kHz, the wave length is

$$\lambda_\mathrm{f} = \frac{\sqrt{K_\mathrm{f}}}{\sqrt{\rho_\mathrm{f}} f} = 0.707 \text{ m}. \tag{26}$$

In contrast, the total length of the fluid chambers including the helicotrema counts just 64.5 mm for the human cochlea. Thus, less than one-tenth of the standing pressure wave resulting from the compression of the fluid fits into the cochlear chambers. Therefore, it is not the compression, but the inertia of the cochlear fluid leading to the pressure difference across the fluid chambers, which in turn excites the characteristic basilar membrane vibration.

5.4. Tonotopy and cochlear gain

Up to this point, the dynamic behavior of the cochlea model is investigated only for one single frequency. In the following, the transfer behavior of this coupled system for different excitation frequencies covering the relevant frequency range for human hearing perception between 100 Hz and 8 kHz is analyzed. This allows us to identify the distribution of the characteristic frequencies along the basilar membrane and thus explains the mechanism which allows the human inner ear to distinguish sounds of different frequencies. Further, the investigations clarify the contribution of the cochlear transfer behavior to the frequency dependence of the auditory threshold.

In Fig. 14, the amplitude of the basilar membrane vibration relative to that of the stapes footplate is shown for different excitation frequencies. Independent of the excitation frequency, all these amplitude responses represent the same characteristics. Starting at the base, the amplitude of the traveling wave increases towards the apex and then reaches a global maximum. Apical to this characteristic position, the amplitude decreases rapidly resulting in an asymmetric amplitude response. However, the characteristic position depends on the excitation frequency. For low excitation frequencies, the amplitude of the traveling wave peaks close to the apex of the cochlea model, whereas for an increased frequency, this characteristic position is shifted towards the base.

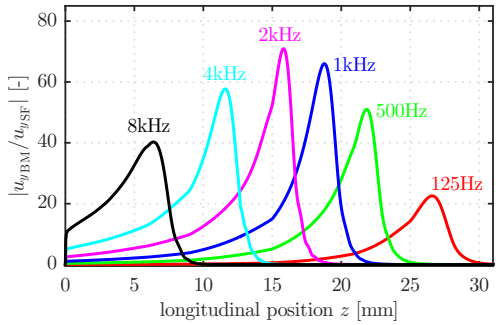

Fig. 14. Amplitude of the basilar membrane relative to that of the stapes shown along the cochlea for different excitation frequencies

As discussed in Section 5.1, the characteristic position correlates with the narrow domain on the basilar membrane, where the stereocilia of the inner hair cells, placed on the basilar membrane, get sheared causing hearing nerve stimulation. The simulation results for the basilar membrane vibration thus clearly demonstrate, that for each single frequency hearing nerves are stimulated primarily in a certain domain of the basilar membrane. This feature of the human cochlea then allows the brain to distinguish between sounds of different frequencies presented at the external ear canal. In this way, the human cochlea acts similar to a discrete frequency analyzer, mapping the excitation frequency to a particular characteristic position on the basilar membrane. This transformation is also called the tonotopy.

For the simulation results in Fig. 14, the corresponding tonotopic map is calculated and shown in Fig. 15. For a logarithmic frequency scale, it becomes evident that the frequencies related to the corresponding characteristic positions are distributed almost logarithmically along the length of the basilar membrane. Even though no direct measurements of the human basilar membrane are provided in literature for validation, this finding is reasonable when compared to psychoacoustic data of humans [57]. Dividing the audible frequency range into 13 so-called critical band widths and correlating these with results of psychoacoustic experiments,

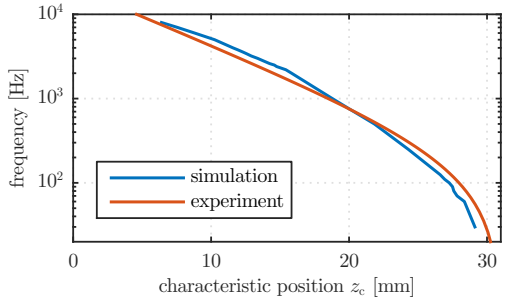

Fig. 15. Tonotopic map calculated from the simulated basilar membrane vibration and compared to psychoacoustic data [57]

the obtained psychoacoustic tonotopic map is in agreement with the numerical result.

Considering once more the amplitude responses for the basilar membrane, Fig. 14, it is notable, that in addition to the shift of the characteristic position also the maximum amplitude changes with the excitation frequency. Since the amplitude of the basilar membrane is shown relative to that of the stapes footplate and thus relative to the excitation, this can be considered as the cochlear gain. As the simulation results clearly indicate, this gain has its maximum at around 2 kHz. This finding agrees well with the transfer behavior of the middle ear, captured from experiments on human temporal bone specimens, indicating a maximum amplification in the same frequency range [49]. Thus, the transfer behavior of both, the inner ear and the middle ear, contribute to the frequency dependence of the auditory threshold, which has its minimum close to 2 kHz for humans [58].

6. Discussion

Compared to other inner ear models published in literature, the FE-model of the human cochlea reported in this paper is unique in two ways. First, the pressure-displacement-based FE formulation is used to describe the flow of the cochlear liquid. With this user-defined element it is not only possible to capture the viscous effects occurring in the cochlear flow, but also to compute the basilar membrane vibration resulting from the fluid-structure interaction in an efficient way. Secondly, the material description of the basilar membrane is more sophisticated compared to other studies. Here, different material formulations for the two zones of the basilar membrane are chosen which is in contrast to the commonly used approach, treating the entire membrane as an isotropic material. Thus this new material description takes the morphologic structure of the basilar membrane into account, whereby the number of material variables required can still be obtained from experimental results provided in literature. Both, the fluid formulation and the material description for the basilar membrane play an important role for the resulting characteristic vibration pattern of the membrane, which in turn results in hearing sensation.

In a first step, the pressure-displacement-based FE formulation for the fluid is validated, Fig. 2. For this purpose, the vibration response of a cantilever beam which is immersed in a viscous fluid is investigated. Thereby, the dimensions and material properties of the fluid-structure coupled system are in a similar range as those of the cochlea. The numerical results for the frequency response are then compared to the analytical solution for the coupled system provided in [18]. Since both results agree well, the user-defined fluid element is capable of accurately describing the cochlear fluid-structure interactions.

In a second step, simulations on the cochlea model are conducted, at first for one single excitation frequency. The simulation results show the formation of a traveling wave on the basilar membrane propagating from the base towards the apex,

www.czasopisma.pan.pl PAN POLSKA AKADEMIA NAUK www.journals.pan.pl

Fig. 6. Thereby, its amplitude increases reaching a maximum at a characteristic position. This in turn leads, mainly in this domain of the membrane, to hearing nerve stimulation. Beyond this point, the amplitude decreases rapidly. Further, the wavelength and thus the velocity of this traveling wave decreases towards the characteristic position, Fig. 7. At the base this velocity is around one order, and close to the characteristic position more than two orders below the velocity of the pressure waves in the fluid demonstrating the introduction of a second time-scale in the cochlea. This way, the simulations provide a deeper understanding for the formation of the traveling wave on the basilar membrane and thus for the generation of hearing nerve stimulation resulting in hearing sensation.

Investigating the calculated fluid velocity field in the vicinity of the basilar membrane, one can identify the damping mechanism leading to the increasing delay of the propagation of the traveling wave. The results clearly show the formation of a viscous boundary layer close to the basilar membrane. In this fluid layer with a thickness of a few micrometers and in particular close to the characteristic position, significant velocity gradients occur, Fig. 10. These in turn lead to extensive viscous damping forces affecting the vibration behavior of the basilar membrane, strongly reducing the velocity and amplitude of the traveling wave. The importance of these viscous damping forces gets particularly evident for lower excitation frequencies, as further investigations show [48]. For lower values of fluid viscosity, the basilar membrane vibration amplitude then no longer totally decays before reaching the apex, which in turn leads to apical reflections and thus resulting in violation of the tonotopy. This way, the investigations demonstrate that the viscosity of the inner ear liquid has a significant impact on the characteristic basilar membrane vibration and thus on hearing sensation. Therefore, an inviscid acoustic fluid formulation is not appropriate to describe the cochlear fluid flow. Further, this justifies in retrospect the choice of the viscous, pressure-displacement-based fluid formulation used in this study.

Furthermore, the study of the velocity distribution across the cochlear chambers allow to classify the cochlear fluid dynamics as a viscous, highly unsteady creeping flow. Thereby the results indicate, that apical to the characteristic position the longitudinal velocity of the liquid is several orders lower compared to the more basal domain and thus, the flow throughout the helicotrema seems negligibly low, at least for higher excitation frequencies, Fig. 11. Thus, the simulations indicate that the coiling of the fluid chambers seems to play a minor role for the cochlear fluid flow.

Compared to classical engineering flow problems, the pressure amplitudes in the cochlear fluid are quite low with a maximum of around 6 Pa, Fig. 12. However, the simulation results for the fluid pressure field in the cochlea clearly indicate that the middle ear leads to an amplification of the pressure presented at the outer ear canal. The maximum pressure amplitude occurs in the basal fluid domain of the vestibulum and scala vestibuli. Due to the low stiffness of the round window membrane, the pressure amplitude is minimal with almost 0 Pa at the basal end

www.czasopisma.pan.pl PAN POLSKA AKADEMIA NAUK www.journals.pan.pl

of the scala tympani. This way, the basilar membrane is subjected to a pressure difference, which in turn evokes the membrane to vibrate, Fig. 13. As the simulation results demonstrate, this pressure difference then decreases towards the apex. Due to the significant vibration amplitude of the basilar membrane at the characteristic position the pressure difference then gets entirely compensated in this domain, rather than at the helicotrema.

The cochlear liquid is slightly compressible. Therefore, in this study, most simulations have been carried out using a compressible fluid description. On the other hand, in order to estimate the influence of compressibility on cochlear dynamics, simulations with an incompressible fluid description were carried out, Fig. 13. These show that it is primarily the inertia of the fluid contributing to the pressure difference across the fluid chambers and thus to the excitation of the basilar membrane leading to hearing sensation instead of the compressibility. The reason for this behavior is that within the relevant frequency range for hearing, the unrolled length of the cochlea chambers is much shorter than the wave length of a standing pressure wave within the slightly compressible cochlear liquid, see also explanations in Section 5.3 and Eq. (26). Consequently, the calculated basilar membrane vibration and its envelope are not significantly affected by the slight compressibility of the cochlear liquid, as further numerical investigations, described in [48], show. Furthermore, this implies that an incompressible fluid description may be used for cochlear modelling in order to describe the fundamental physical effects occurring in the cochlea.

Finally, the transfer behavior of the FE-model of the human cochlea is investigated for different excitation frequencies. The simulation results show that the amplitude of the traveling wave on the basilar membrane peaks at a frequency dependent characteristic position along the cochlea, Fig. 14. Mainly in this domain hearing nerves are stimulated. For low excitation frequencies, this position is close to the apex, whereas for increasing frequencies this point is shifted towards the base. In this way, for each single frequency hearing nerves primarily in a certain domain of the basilar membrane are stimulated and the human cochlea apparently acts similarly to a discrete frequency analyzer. This transformation is also called the tonotopy. This way, the simulations explain the capability of the human inner ear to distinguish sounds of different frequencies. Analyzing the tonotopic map of the human cochlea model, it is obvious that the characteristic frequencies are distributed logarithmically along the basilar membrane, Fig. 15. This agrees well with psychoacoustic observation for humans provided in [57]. The developed FE-model clearly shows the formation of a traveling wave on the basilar membrane, which is observed also in measurements [51, 52]. Therefore, the model is able to represent the fundamental physical effects occurring in the human cochlea. Although the basilar membrane vibration can be validated quantitatively only in a very few points based on measurements provided in [53], the dynamic behavior for these single points fits quite well. Since the parameters of this physical model were not tuned to these few validation points and the material description of the

www.czasopisma.pan.pl PAN POLSKA AKADEMIA NAUK www.journals.pan.pl

basilar membrane is based on its real morphologic structure, it can be assumed that the developed FE-model captures the real basilar membrane vibration behavior in other points too.

Further, it can be seen from the simulations that the maximal amplitude of the traveling wave relative to that of the stapes changes with frequency as well, Fig. 14. This so-called cochlear gain has its maximum around 2 kHz. Thus, not only the middle ear, but also the inner ear transfer behavior contributes to the frequency dependence of the auditory threshold having its minimum in the same frequency range for humans.

7. Conclusion

A deeper understanding of the fluid dynamics and the resulting vibration of the basilar membrane in the cochlea, which in turn leads to hearing nerve stimulation, is of central interest. However, measurements within this closed hydraulic system with its complex geometry and delicate structures only provide a limited insight into the cochlear dynamics. Therefore, in this study, a three-dimensional FE-model of the intact human cochlea with a simplified geometry is developed to simulate the fundamental physical effects occurring in this coupled system.

In contrast to previous inner ear models published in literature, here a two-zone orthotropic material description is introduced for the basilar membrane based on its morphologic structure and an user-defined pressure-displacement-based fluid element is used to describe the flow of the cochlear liquid. In contrast to acoustic elements, this fluid formulation allows one to capture the viscous forces in the fluid and enables a numerically stable and efficient calculation of the cochlear fluid-structure interactions compared to the commonly used partitioned approach.

The developed model allows one to predict the fluid flow in the human cochlea and its interaction with the basilar membrane. The cochlear flow, which evokes the basilar membrane vibration, is highly unsteady and viscous. Since the employed fluid formulation also captures the viscous forces, the simulations allow us to identify and understand the damping mechanism leading to the formation of this characteristic wave. This traveling wave on the basilar membrane then finally results in hearing nerve stimulation in a frequency dependent domain. Thus, the cochlea acts similarly to a discrete frequency analyzer and the calculated tonotopic map agrees well with psychoacoustic measurements. Further the results indicate, that the calculated transfer behavior of the cochlea does not compensate, but contributes to the frequency dependence of the human auditory threshold. This way, the presented FE-model allows one to gain deeper insights into the physical effects occurring in the human cochlea and the simulation results significantly contribute to a deeper understanding of the development of hearing sensation in an intact cochlea.

Since the developed model is based on physical parameters, small geometric modifications will allow us to simulate pathological changes on hearing sensation. This will help to clarify how inner ear diseases, such as semicircular dehiscence

www.czasopisma.pan.pl PAN POLSKA AKADEMIA NAUK www.journals.pan.pl

or endolymphatic hydrops, affect the auditory system. Comparing these results with those of the intact cochlea model, this may also allow one to derive new diagnostic methods. Additionally, the implementation of passive hearing implants is conceivable in order to develop innovative hearing aids, which will be the concern of future studies.

Acknowledgements

The authors thank Dr.-Ing. J. Baumgart, MPI for the Physics of Complex Systems, and Dr.-Ing. M. Fleischer, University Dresden, for providing the user-defined element implemented in ANSYS and for interesting discussions.

Manuscript received by Editorial Board, July 27, 2020;
final version, November 11, 2020.

References

[1] L. Robles and M.A. Ruggero. Mechanics of the mammalian cochlea. *Physiological Reviews*, 81(3):1305–1352, 2001. doi: 10.1152/physrev.2001.81.3.1305.

[2] M. Fleischer. Mehrfeldmodellierung und Simulation der äußeren Haarsinneszelle der Cochlea (Multifield modelling and simulation of the outer hair cells of the cochlea). Doctoral Thesis. Technische Universität Dresden, Germany, 2012. (in German).

[3] J. Baumgart. The hair bundle: Fluid-structure interaction in the inner ear. Doctoral Thesis. Technische Universität Dresden, Germany, 2010.

[4] J. Tian, X. Huang, Z. Rao, N. Ta, and L. Xu. Finite element analysis of the effect of actuator coupling conditions on round window stimulation. *Journal of Mechanics in Medicine and Biology*, 15(4):1–19, 2015. doi: 10.1142/S0219519415500487.

[5] R.Z. Gan, B.P. Reeves, and X. Wang. Modeling of sound transmission from ear canal to cochlea. *Annals of Biomedical Engineering*, 35:2180–2195, 2007. doi: 10.1007/s10439-007-9366-y.

[6] L. Xu, X. Huang, N. Ta, Z. Rao, and J. Tian. Finite element modeling of the human cochlea using fluid-structure interaction method. *Journal of Mechanics in Medicine and Biology*, 15(3):1–13, 2015. doi: 10.1142/S0219519415500396.

[7] H.W. Ades and H. Engström. Anatomy of the inner ear. In: Keidel W.D., Neff W.D. (eds) *Auditory System. Handbook of Sensory Physiology*, vol. 5/1. Springer, Berlin, 1974. doi: 10.1007/978-3-642-65829-7_5.

[8] C.R. Steele, G.J. Baker, J.A. Tolomeo, and D.E. Zetes-Tolometo. Cochlear mechanics. In: J.D. Bronzino (ed.) *The Biomedical Engineering Handbook*, CRC Press, 2006.

[9] S. Iurato. Functional implications of the nature and submicroscopic structure of the tectorial and basilar membranes. *The Journal of the Acoustical Society of America*, 34(9):1386–1395, 1962. doi: 10.1121/1.1918355.

[10] H. Herwig. *Strömungsmechanik: Einführung in die Physik von technischen Strömungen (Introduction to the Physics of Technical Flows)*. Springer Vieweg, Wiesbaden; 2008. (in German).

[11] H. Schlichting and K. Gersten. *Boundary-Layer Theory*, vol. 7. Springer-Verlag, Berlin, 2017.

[12] G.H. Keulegan and L.H. Carpenter. Forces on cylinders and plates in an oscillating fluid. *Journal of Research of the National Bureau of Standards*, 60:423–440, 1958.

[13] E. Zwicker. Über die Viskosität der Lymphe im Innenohr des Hausschweines (About the viscosity of the lymph in the inner ear of the domestic pig). *Acta Otolaryngologica*, 78(1-6): 65–72, 1974. (in German). doi: 10.3109/00016487409126327.

www.czasopisma.pan.pl PAN POLSKA AKADEMIA NAUK www.journals.pan.pl

[14] M. Lesser and D. Berkley. Fluid mechanics of the cochlea. Part 1. *Journal of Fluid Mechanics*, 51(3):497–512, 1972. doi: 10.1017/S0022112072002320.

[15] A. De Paolis, H. Watanabe, J. Nelson, M. Bikson, M. Marom, M. Packer, and L. Cardoso. Human cochlear hydrodynamics: A high-resolution μCT-based finite element study. *Journal of Biomechanics*, 50:209–216, 2017. doi: 10.1016/j.jbiomech.2016.11.020.

[16] L. Papula. *Mathematische Formelsammlung (Mathematical Formula Collection)*. Springer Verlag, Wiesbaden, 2014. (in German).

[17] O.C. Zienkiewicz, R.L. Taylor, and J.Z. Zhu. *The Finite Element Method: Its Basis and Fundamentals*, 6 ed. Elsevier Butterworth-Heinemann, Oxford, 2006.

[18] J.E. Sader. Frequency response of cantilever beams immersed in viscous fluids with applications to the atomic force microscope. *Journal of Applied Physics*, 84(1):64–76, 1998. doi: 10.1063/1.368002.

[19] E. de Boer. Auditory physics. Physical principles in hearing theory. Part 1. *Physics Reports*, 62(2):87–174, 1980. doi: 10.1016/0370-1573(80)90100-3.

[20] M.J. Wittbrodt, C.R. Steele, and S. Puria. Developing a physical model of the human cochlea using microfabrication methods. *Audiology and Neurotology*, 11(2):104–112, 2006. doi: 10.1159/000090683.

[21] C.R. Steele and J.G. Zais. Effect of coiling in a cochlear model. *The Journal of the Acoustical Society of America*, 77(5):1849–1852, 1985. doi: 10.1121/1.391935.

[22] J. Wysocki. Dimensions of the human vestibular and tympanic scalae. *Hearing Research*, 135(1-2):39–46, 1999. doi: 10.1016/S0378-5955(99)00088-X.

[23] M. Thorne, A.N. Salt, J.E. DeMott, M.M. Henson, O.W. Henson, and S.L. Gewalt. Cochlear fluid space dimensions for six species derived from reconstructions of resonance images. *Annals of Otology, Rhinology & Laryngology*, 109(10):1661–1668, 1999. doi: 10.1097/00005537-199910000-00021.

[24] G. Herrmann and H. Liebowitz. *Mechanics of Bone Fractures*. Academic Press, New York, 1972.

[25] J. Kirikae. *The Middle Ear*. Tokyo: University of Tokyo Press, 1960.

[26] F. Atturo, M. Barbara, and H. Rask-Andersen. Is the human round window really round? An anatomic study with surgical implications. *Otology and Neurotology*, 35(8):1354–1360, 2014. doi: 10.1097/MAO.0000000000000332.

[27] M.V. Goycoolea and L. Lundman. Round window membrane. Structure, function and permeability. A review. *Microscopy Research and Technique*, 36(3):201–211, 1997. doi: 10.1002/(SICI)1097-0029(19970201)36:3<201::AID-JEMT8>3.0.CO;2-R.

[28] M. Kwacz, M. Mrówka, and J. Wysocki. Round window membrane motion before and after stapedotomy surgery. An experimental study. *Acta of Bioengineering and Biomechanics*, 13(3):27–33, 2011.

[29] X. Zhang and R.Z. Gan. Dynamic properties of human round window membrane in auditory frequencies running head: Dynamic properties of round window membrane. *Medical Engineering & Physics*, 35(3):310–318, 2013. doi: 10.1016/j.medengphy.2012.05.003.

[30] A.A. Poznyakovskiy, T. Zahnert, Y. Kalaidzidis, N. Lazurashvili, R. Schmidt, H.J. Hardtke, B. Fischer, and Y.M. Yarin. A segmentation method to obtain a complete geometry model of the hearing organ. *Hearing Research*, 282(1-2):25–34, 2011. doi: 10.1016/j.heares.2011.06.009.

[31] P. Leichsenring. Aufbereitung von Geometriedaten der menschlichen Cochlea (Preparation of geometry data for the human cochlea). Master Thesis. Technische Universität Dresden, Germany, 2012. (in German).

[32] E.G. Wever. The width of the basilar membrane in man. *Annals of Otology, Rhinology & Laryngology*, 47:37–47, 1938.

www.czasopisma.pan.pl PAN POLSKA AKADEMIA NAUK www.journals.pan.pl

[33] F. Böhnke. Finite Elemente Analysen zur Berechnung der Signalverarbeitung in der Cochlea (Analyses for computation of signal processing in the cochlea). Doctoral Thesis. Technische Universität Ilmenau, Germany, 1999. (in German).

[34] L.M. Cabezudo. The ultrastructure of the basilar membrane in the cat. *Acta Oto-Laryngologica*, 86(1-6):160–175, 1978. doi: 10.3109/00016487809124733.

[35] S. Newburg, A. Zosuls, P. Barbone, and D. Mountain. Mechanical response of the basilar membrane to lateral micromanipulation. In: *Concepts and Challenges in the Biophysics of Hearing. Proceedings of the 10th International Workshop on the Mechanics of Hearing*, pages 240–246, 2009. doi: 10.1142/9789812833785_0038.

[36] V. Tsuprun and P. Santi. Ultrastructure and immunohistochemical identification of the extracellular matrix of the chinchilla cochlea. *Hearing Research*, 129(1-2):35–49, 1999. doi: 10.1016/S0378-5955(98)00219-6.

[37] I.U. Teudt and C.P. Richter. The hemicochlea preparation of the guinea pig and other mammalian cochleae. *Journal of Neuroscience Methods*, 162(1-2):187–197, 2007. doi: 10.1016/j.jneumeth.2007.01.012.

[38] M. Fleischer, R. Schmidt, and A.W. Gummer. Compliance profiles derived from a three-dimensional finite-element model of the basilar membrane. *The Journal of the Acoustical Society of America*, 127(5):2973–2991, 2010. doi: 10.1121/1.3372752.

[39] J. Baumgart, M. Fleischer, and C. Steele. The traveling wave in the human inner ear studied by means of a finite-element model including middle and outer ear. In: *Proceedings of the 23rd International Congress on Sound & Vibration*, Greece, 2016.

[40] H. Altenbach, J.W. Altenbach, and W. Kissing. *Mechanics of Composite Structural Elements*. Springer-Verlag, Berlin, 2013.

[41] R.C. Naidu and D.C. Mountain. Basilar membrane tension calculations for the gerbil cochlea. *The Journal of the Acoustical Society of America*, 121(2):994–1002, 2007. doi: 10.1121/1.2404916.

[42] S. Liu and R.D. White. Orthotropic material properties of the gerbil basilar membrane. *The Journal of the Acoustical Society of America*, 123(4):2160–2171, 2008. doi: 10.1121/1.2871682.

[43] C.E. Miller. Structural implications of basilar membrane compliance measurements. *The Journal of the Acoustical Society of America*, 77(4):146–1474, 1985. doi: 10.1121/1.392041.

[44] L. Schweitzer, C. Lutz, M. Hobbs, and S.P. Weaver. Anatomical correlates of the passive properties underlying the developmental shift in the frequency map of the mammalian cochlea. *Hearing Research*, 97(1-2):84–94, 1996. doi: 10.1016/S0378-5955(96)80010-4.

[45] R.C. Naidu and D.C. Mountain. Measurements of the stiffness map challenge. A basic tenet of cochlear theories. *Hearing Research*, 124(1-2):124–131, 1998. doi: 10.1016/S0378-5955(98)00133-6.

[46] H. Wada and T. Kobayashi. Dynamical behavior of middle ear: Theoretical study corresponding to measurement results obtained by a newly developed measuring apparatus. *The Journal of the Acoustical Society of America*, 87(1):237–245, 1990. doi: 10.1121/1.399290.

[47] M. Kwacz, P. Marek, P. Borkowski, and M. Mrówka. A three-dimensional finite element model of round window membrane vibration before and after stapedotomy surgery. *Biomechanics and Modeling in Mechanobiology*, 12:1243–1261, 2013. doi: 10.1007/s10237-013-0479-y.

[48] P. Wahl. Simulation der Fluidströmung und Basilarmembranschwingung im menschlichen Innenohr (Simulation of fluid flow and basilar membrane vibrations in the human inner ear). Doctoral Thesis. Universität Stuttgart, Germany, 2018. (in German).

[49] J.H. Sim, M. Chatzimichalis, M. Lauxmann, C. Röösli, A. Eiber, and A. Huber. Complex stapes motion in human ears. *Journal of the Association for Research in Otolaryngology*, 11(3):329–341, 2010. doi: 10.1007/s10162-010-0207-6.

www.czasopisma.pan.pl PAN POLSKA AKADEMIA NAUK www.journals.pan.pl

[50] S. Huang and E.S. Olson. Auditory nerve excitation via a non-traveling wave mode of basilar membrane motion. *Journal of the Association for Research in Otolaryngology*, 12:559-575, 2011. doi: 10.1007/s10162-011-0272-5.

[51] G. von Békésy. *Experiments in Hearing*. McGraw-Hill, New York, 1960.

[52] T.Ren. Longitudinal pattern of basilar membrane vibration in the sensitive cochlea. *Proceedings of the National Academy of Sciences*, 99(26):17101–17106, 2002. doi: 10.1073/pnas.262663699.

[53] S. Stenfelt, S. Puria, N. Hato, and R.L. Goode. Basilar membrane and osseous spiral lamina motion in human cadavers with air and bone conduction stimuli. *Hearing Research*, 181(1-2): 131–143, 2003. doi: 10.1016/S0378-5955(03)00183-7.

[54] S. Ramamoorthy, N.V. Deo, and K. Grosh. A mechano-electro-acoustical model for the cochlea: response to acoustic stimuli. *The Journal of the Acoustical Society of America*, 121(5): 2758–2773, 2007. doi: 10.1121/1.2713725.

[55] W.E. Langlois and M.O. Deville. *Slow Viscous Flow*. 2nd ed. Springer, Cham, 2014. doi: 10.1007/978-3-319-03835-3.

[56] E. Olson. Direct measurement of intra-cochlear pressure waves. *Nature*, 402:526–529, 1999. doi: 10.1038/990092.

[57] D.D. Greenwood. A cochlear frequency-position function for several species – 29 years later. *The Journal of the Acoustical Society of America*, 87(6):2592–2605, 1990. doi: 10.1121/1.399052.

[58] H.G. Boenninghaus and T. Lenarz. *HNO: Hals-Nasen-Ohrenheilkunde (Otorhinolaryngology)*. Springer, Berlin, 2007. (in German).